



CHORUS

This is the accepted manuscript made available via CHORUS. The article has been published as:

Local probing of nuclear bath polarization with a single electronic spin

P. London, R. Fischer, I. Alvizu, J. R. Maze, and D. Gershoni

Phys. Rev. B **92**, 241117 — Published 28 December 2015

DOI: [10.1103/PhysRevB.92.241117](https://doi.org/10.1103/PhysRevB.92.241117)

Local probing of nuclear bath polarization with a single electronic spin

P. London,^{1,*} R. Fischer,¹ I. Alvizu,² J. R. Maze,² and D. Gershoni¹

¹*Department of Physics, Technion, Israel Institute of Technology, Haifa 3200003, Israel and*

²*Departamento de Física, Pontificia Universidad Católica de Chile, Santiago 7820436, Chile*

The effect of a polarized nuclear spin bath on the dynamical behavior of a single electronic spin is studied theoretically and experimentally; The polarization of a single nuclear spin modifies the spin-echo signal of its neighboring electronic spin. When the electronic spin is surrounded by a bath of polarized nuclei, the spin-echo signals manifest a characteristic frequency related only to the nuclear spins abundance and their collective polarization. This frequency is proposed as a novel indicator for the local nuclear bath polarization. We quantify the realistic experimental regimes at which the scheme is efficient. Our proposal has potential applications for quantum sensing schemes, and opens a route for a systematic study of polarized mesoscopic-systems.

Enhancement of nuclear polarization via polarization transfer from electronic spins is a basic ingredient in nuclear magnetic resonance (NMR) science, and a promising approach for enhancing the sensitivity of nuclear spin based applications, such as magnetic resonance imaging (MRI). For quantum information processing (QIP) and quantum metrology studies, nuclear bath polarization is essential for initializing the state of the system, for instance in a quantum simulator¹, or for increasing the signal-to-noise ratio (SNR)²⁻⁴. However, measuring the polarization of nuclear spins is a challenge due to their tiny magnetic moment. Possible solutions tackling this difficulty are measurements involving large ensembles^{5,6}, or the search for electronic spins energy shifts due to static nuclear spin polarization⁷⁻⁹. An additional approach is to probe the influence of the nuclear polarization on the **dynamical** behavior of a central electronic spin. In¹⁰⁻¹³, the dephasing and decoherence properties of an electronic spin were shown to be connected with the polarization of its surrounding bath. Interestingly, if dynamical decoupling is applied, also the coherent evolution of the spin is effected by the polarization¹⁴.

Here, we analyze the effect of nuclear bath polarization on a prototypical central spin system - the nitrogen-vacancy (NV) color center in diamond interacting with a bath of ¹³C nuclear spins. The NV-center in diamond is a promising physical platform for QIP and nanoscale metrology; its ground state sub-levels are optically accessible, can be coherently manipulated using MW fields, and present unprecedentedly long coherence times for a solid state system at room-temperature¹⁵. These properties have engaged a number of important NV-center demonstrations in QIP¹⁶, nanoscale magnetometry^{17,18}, nanoscale NMR^{2,3}, and measurements in living cells^{19,20}. We study the dynamics of the NV-center interacting with a polarized nuclear environment under the simplest, yet powerful, dynamical decoupling protocol - the spin-echo sequence²¹. We propose the electronic spin coherent evolution as a novel measuring method for its surrounding bath polarization, and compare with free induction decay (FID) based techniques.

An illustration of the model system is given in Fig.1a; It comprises the electronic spin of an NV-center, and an

ensemble of nuclear spins randomly distributed in a diamond lattice in the presence of an external magnetic field **B**. The experimental pulse sequence is given in Fig.1b. In spin-echo measurement a $(\pi/2)$ pulse rotates the initialized state $|0\rangle$ to a $(1/\sqrt{2})[|0\rangle + |1\rangle]$ superposition, $\{|0\rangle, |1\rangle\}$ being the basis of the electronic spin in the absence of a nuclear bath. This superposition accumulates dynamical phase according to the local magnetic field at the electronic-spin position²², but tends to decohere after a short time, T_2^* . An additional π pulse after a duration τ will result with a revival of the electronic coherence, S , after an identical duration²¹. A biased magnetic field (one which is not identical in both parts of the sequence) causes the spin to accumulate phase, and to serve as AC-magnetometer²³. In what follows, we show that surrounding nuclear polarization imitates this effect, as the electronic spin itself changes the nuclear bath in an unbalanced fashion. To distinguish between decoherence of the spin ($|S| < 1$) and phase accumulation, we use *Quadrature detection*, i.e. reconstruction of the **magnitude and phase** of the coherence. In an NV-based measurement, an additional $(\pi/2)$ pulse rotates the electronic coherence into an optically-measurable population-difference of the ground state sublevels, and quadrature detection is achieved by extracting the real component from an in-phase (I) pulses sequence $(\frac{\pi}{2})_x \frac{\tau}{\tau} (\pi)_x \frac{\tau}{\tau} (\frac{\pi}{2})_x$, and the imaginary component from the out-of-phase (Q) sequence $(\frac{\pi}{2})_x \frac{\tau}{\tau} (\pi)_x \frac{\tau}{\tau} (\frac{\pi}{2})_y$ ^{24,25} (Fig. 1b). Using density matrix formalism, the coherence can be written as $S = \prod_k S_k$, where²⁶⁻²⁹

$$S_k = \text{Tr}_{nuc} \left(U_1^{k\dagger} U_0^{k\dagger} U_1^k U_0^k \rho_k \right). \quad (1)$$

Here, $U_{m_s}^k = \exp(-iH_{m_s}^k \tau)$ represents the evolution operator of the k-th nuclear spin conditioned by the electron spin state m_s , and $H_{m_s}^k = \frac{\omega_{m_s}^k}{2} \vec{\sigma}^k \cdot \hat{\mathbf{n}}_{m_s}^k$ is its corresponding Hamiltonian, where $\vec{\sigma}^k$ are the Pauli matrices vector of the k-th nuclear spin, and $\omega_{m_s}^k \hat{\mathbf{n}}_{m_s}^k = \gamma_n \mathbf{B} + m_s \mathbf{A}_k$. Here, the vector \mathbf{A}_k characterizes the interaction between the k-th nuclear spin and the electronic spin under the secular approximation. Finally, ρ_k in Eq. (1) is a density matrix characterizing the initial state of the k-th nuclear

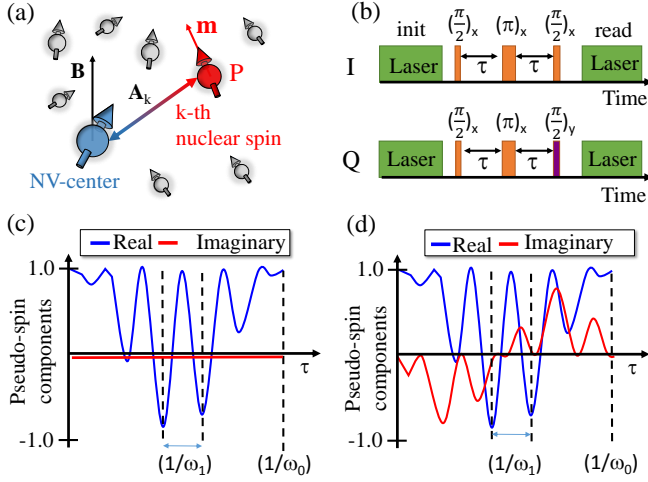


Figure 1: Spin-echo measurement in the presence of a polarized nuclear spin. (a) A single electronic spin interacts with a bath of nuclear spins subject to an external magnetic field (b) Schematic description of the spin-echo pulse sequence. I - in-phase sequence, Q - out-of-phase sequence. (c)[(d)] The pseudo spin (S) components as calculated from Eq.(2) using $\omega_1 = 6\omega_0$ for unpolarized [polarized] nuclear spin ; The real value is obtained by the in-phase sequence (I), and the imaginary values are obtained by the out-of-phase sequence (Q).

spin. We note that $\omega_{m_s=0}$ and $\hat{\mathbf{n}}_{m_s=0}$ are common to all nuclear spins.

The dynamics reflected from Eq.(1) was previously considered and measured^{29–31}, under the assumption that the nuclear spin-bath is unpolarized, $\rho_k = \frac{1}{2}\mathbf{1}$ (*high temperature limit*). The focus of this work is to introduce polarization to the nuclear system, and to investigate its influence on the dynamical behavior of the electronic spin NV-center. Describing the average of many bath spin realizations, we introduce the nuclear bath polarization as a non-coherent state, $\prod_k \rho_k$, where $\rho_k = \frac{1}{2}\mathbf{1} + \frac{P_k}{2}\sigma^k \cdot \hat{\mathbf{n}}_0$, P_k being the projection of the k -th nuclear spin polarization on the external field axis ($-1 \leq P_k \leq 1$). In this case, the total averaged nuclear polarization is $(\sum P_k)\hat{\mathbf{n}}_0$ (See details on this description in the supplementary information²⁵)

For a single (k -th) nuclear spin, Eq.(1) can be expressed explicitly

$$S_k = 1 - |\hat{\mathbf{n}}_0 \times \hat{\mathbf{n}}_1^k|^2 \sin^2\left(\frac{\omega_1^k \tau}{2}\right) \times (\cos(\omega_0 \tau) - iP_k \sin(\omega_0 \tau) - 1). \quad (2)$$

The spin-echo envelope modulation formula^{27,32} is given by the real part of Eq. (2), and is independent of the nuclear spin state. In contrast, the imaginary part of S_k is proportional to the polarization P_k . Fig.1c, and Fig.1d depict the temporal evolution of both S_k components for the unpolarized and polarized case, respectively.

To validate the predictions of our theory, we performed experiments with a single NV center interacting with a

single ^{13}C whose polarization is controlled at will, and is measured in an orthogonal way to our proposed scheme. The system is represented with the electron spin states $|0\rangle, |1\rangle$ and with the nuclear spin states $|\alpha_{\pm}\rangle$ which are the eigen-states of $H_{m_s=1}$ (Fig. 2a). It has a characteristic splitting $\Delta = (2\pi)9\text{MHz}$ between the nuclear states within the $|1\rangle$ manifold, and rotation frequency $\delta = (2\pi)0.06\text{MHz}$ between the nuclear states within the $|0\rangle$ manifold (determined by our magnetic field alignment). Fig. 1b schematically describes the three principle steps in the experiment: A long laser pulse polarizes the electron spin and depolarizes the nuclear spin³³ (step 1). Then, MW and optical pumping operations are synchronized with the rotation δ to efficiently polarize the nuclear spin to one of the $|\alpha_{\pm}\rangle$ ³⁴ (step 2, for details on our experimental parameters see²⁵). Finally, the I or Q echo sequences are employed, and are followed by a readout laser (step 3). Fig. 2c presents the measured spin-echo I, Q signals, when the nuclear spin was either polarized or remained unpolarized (denoted pol and ref, respectively). The collapse of electron spin coherence is accompanied with a fast modulation at Δ frequency, as predicted by Eq. (2) (Fig2c, I-signals). The same frequency appears in the Q-signal only if the nuclear spin is initially polarized. For a signal S (I, or Q), the Fourier spectrum $F_S(\omega)$ helps to quantify the effect. Specifically, $F_Q(\Delta)$ is the amplitude of the modulation (Fig.2d, starred peak) which indicates the degree of nuclear polarization. The Fourier components of the I-signal and Q-signal share common parameters which can be eliminated by looking at a normalized observable $\eta = F_Q(\Delta)/F_I(\Delta)$ [Fig.2e-f]. For this strongly coupled spin, one has a direct measurement of the nuclear polarization: during free evolution, the nuclear state precesses between the $|\alpha_{\pm}\rangle$ states periodically³⁵. This precession can be observed with a MW π -pulse and laser readout, and its amplitude is proportional to the nuclear polarization, P . In our experiments, we polarized the nuclear spin to its $|\alpha_{-}\rangle$ state and measured the nuclear polarization using both techniques, i.e. our quadrature spin-echo technique and the direct method. The former gives η , and the latter gives P [Fig. 2e]. (The starred point in Fig.2e represents the data extracted from the Q-signal curve in Fig.2d, which is marked by a star). When a laser pulse of various durations was applied between the nuclear polarization step and the nuclear polarization measurement step (Fig.2e, inset), we have observed a gradual decrease in the nuclear polarization³³ (Fig.2e), and established the relation $P \simeq \eta$ (black line in Fig.2e is the ideal relation). Moreover, we have used the precession between the $|\alpha_{\pm}\rangle$ states to characterize the dependence of the Q-signal in the polarization direction (Fig.2f, inset). Performing the quadrature detection at various times, we find a strong modulation of the Q-signal as the nuclear spin rotates prior to the spin-echo measurement (Fig.2f). Numerical propagation of Eq.(1) reproduces these results when the initial nuclear density matrix ρ_k is introduced to the simulation according to free precession of the coherent

nuclear superposition $|\alpha_{-}\rangle$ state around \mathbf{B} (Fig. 2f, red line).

We now show that the polarization of a nuclear spin bath in the NV-center surrounding can be extracted from this protocol. As each of the S_k terms in Eq.(1) is a complex number, the calculation of the total pseudo-spin S is merely a multiplication of their amplitude and a

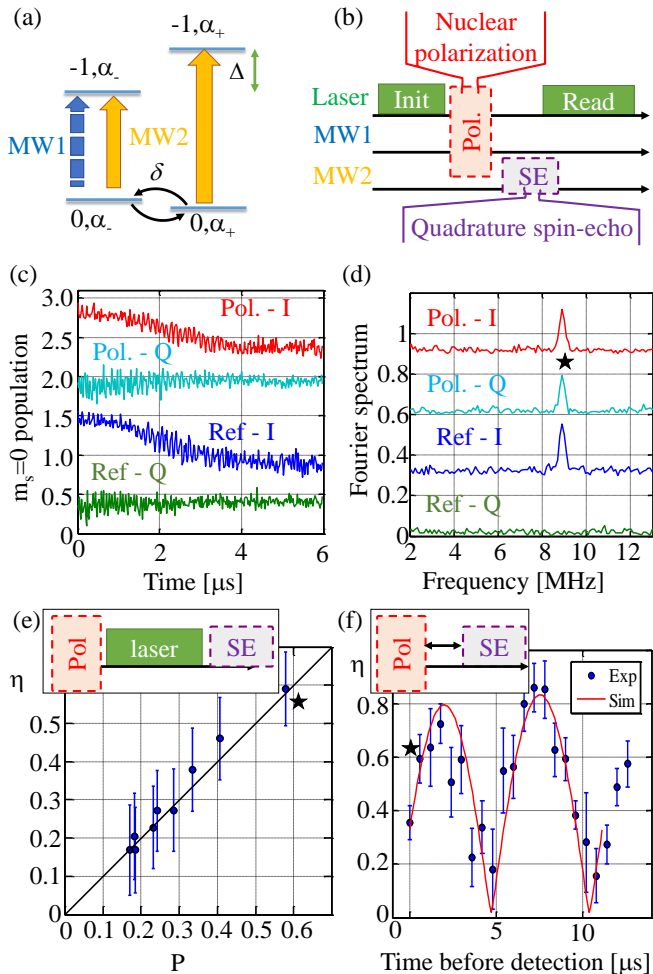


Figure 2: Demonstration of nuclear polarization effect on spin-echo. (a) Energy levels and states of the electronic ($|0\rangle, |-1\rangle$) and nuclear ($|\alpha_{\pm}\rangle$) spins. MW1 - a resonant MW field which acts on the $|0\alpha_{-}\rangle$ level only (dashed blue arrow). MW2 - a MW field which acts on both levels (solid orange arrows). (b) The experimental steps (see main text). (c) Measured quadrature spin-echo signals (Pol. - polarized nuclear spin, Ref. - unpolarized nuclear spin). (d) Fourier spectra of the signals in (c). (e) The polarization observable η (defined in the main text) as a function of the nuclear spin polarization. The inset illustrates the addition of a laser pulse used to destruct the nuclear polarization. The data point marked by star corresponds to the measurement in (d). (f) η as a function of the temporal delay between the nuclear polarization step and spin-echo measurement, as schematically described in the inset. The solid red curve represent theoretical simulations (see text).

summation of their phase, giving $S = \Lambda(t) e^{i\Phi(t)}$ where $\Lambda(t)$ has the ‘‘collapse and revival’’ character³² and

$$\Phi(\tau) = \sum_k \tan^{-1} \left(P_k \frac{C_0}{S_0} \frac{2 |\hat{\mathbf{n}}_0 \times \hat{\mathbf{n}}_1^k|^2 S_0^2 (S_1^k)^2}{2 |\hat{\mathbf{n}}_0 \times \hat{\mathbf{n}}_1^k|^2 S_0^2 (S_1^k)^2 - 1} \right). \quad (3)$$

Here, $S_{0(1)} = \sin(\frac{\omega_{0(1)}\tau}{2})$ and $C_{0(1)} = \cos(\frac{\omega_{0(1)}\tau}{2})$. Importantly, though each nuclear spin possesses only a small imaginary term, the total angle, being the sum of many nuclear spins, can be finite. This leads to the characteristic behavior illustrated in Fig.3a. Here, the oscillations of the S components (essentially, a rotation of S in the complex plane) are seen at the revival times. In contrast to the single nuclear spin case (Fig.1c,d), in the polarized bath case the I -signal is modified by the polarized nuclear bath, in addition to the dramatic change in the Q -signal. At the revival times ($\omega_0 t_r \simeq 2\pi$), the phase accumulation rate can be approximated as

$$\varpi = \left. \frac{d\Phi(t)}{dt} \right|_{t_r} \simeq -\frac{\omega_0}{2} \sum_k |\hat{\mathbf{n}}_0 \times \hat{\mathbf{n}}_1^k|^2 P_k. \quad (4)$$

At the revival times, ϖ correlates with the total magnetization in the NV-center surroundings. The weighting factor $|\hat{\mathbf{n}}_0 \times \hat{\mathbf{n}}_1^k|^2$ ensures convergence of the sum and expresses the importance of nearby nuclear spins (alternatively quantify at which magnetic field one should expect a prominent signal)³⁶. Therefore, we propose to use ϖ as a quantitative measurement for the effective magnetization in the NV-center vicinity. Since the oscillations are only observed during the revival time of the spin-echo modulation, the revival duration ΔT influences the oscillations contrast C roughly as $C \simeq \exp[-(\frac{\pi}{\varpi \Delta T})^2]$, and determines a lower limit for the detectable magnetization.

In our simulations, nuclear spins were randomly positioned in their lattice sites yielding a desired ^{13}C abundance. A hollow-sphere configuration was used ($0.65\text{nm} \leq R \leq 5.5\text{nm}$) for omitting the strongly coupled nuclear spins; these spins are not described adequately by the dipole term taken in Eq.(1), since their hyperfine interaction mixes the electron and nuclear states³². Moreover, these spins introduce high-frequency components into the signal (and consequently to 3), thus obscure the universal behavior of an NV-center surrounded by a polarized bath. Fig. 3b shows the simulated Q -signals at a magnetic field of $B = 10$ G and natural ^{13}C abundance ($n = 0.01$). We note that ϖ depends linearly on the polarization P , in agreement with Eq.(4), thus could serve as a bath polarization indicator. Fig.3c summarizes the influence of the physical regime (magnetic fields and ^{13}C abundances) on the observable ϖ , and illustrates the dependence of this phenomenon in the weighting factors $|\hat{\mathbf{n}}_0 \times \hat{\mathbf{n}}_1^k|^2$. The total effect is quenched by increasing the magnetic field, and grows with the number of contributing nuclear spins. Fig.3d depicts the contrast

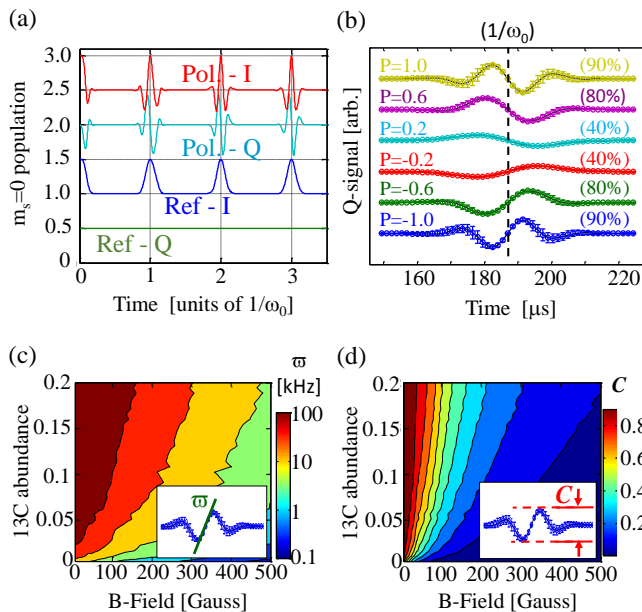


Figure 3: Characteristic frequencies in polarized-bath spin-echo signal. (a) Simulated quadrature spin-echo signals (Pol. - polarized nuclear bath, Ref. - unpolarized nuclear bath). We used $B = 50$ G, $n = 0.1$, and $P = 1$ for the polarized bath case (b) The Q-signals at the first revival time for various degree of polarization ($B = 10$ G, $n = 0.01$). (c,d) The frequency ϖ and the contrast C as a function of the magnetic field B , and ^{13}C abundance n , for a maximally polarized nuclear spin environment ($P=1$).

C of the revival signal versus the ^{13}C abundance and the ambient magnetic field, and assists in evaluating the scheme's efficiency. Observable signal is expected at relatively low magnetic fields $B \leq 50$ G, even for diamonds with natural ^{13}C abundance (for example, $\varpi=50$ kHz and $C=90\%$, at $B = 5$ G, $n = 0.01$). At magnetic fields of $B = 500$ G, $\hat{\mathbf{n}}_0 \times \hat{\mathbf{n}}_1^k$ are relatively small and accordingly ϖ is small. For higher ^{13}C concentrations, however, the expected contrast is $C \sim 10\%$, and the corresponding frequency is $\varpi \sim 10$ kHz. The latter regime is particularly interesting because it promotes nuclear-bath polarization through excited-state level anti-crossing method^{5,37,38}).

To conclude, we studied the use of a central spin, realized here by the NV-center, as a probe for the polarization of a proximal spin bath. We demonstrated experimentally that by measuring the time dependence of the spin-echo quadrature one can determine the polarization magnitude of a vicinal nuclear spin, and learn about its orientation too. In the case of a polarized spin bath we found that the electronic coherence rotates in a characteristic frequency, which is proportional to the average bath magnetization. Thus, our scheme offers a novel sensing method for mesoscopic polarized environments. Our sensing method is insensitive to the nuclei

geometrical configuration, in contrast to the Zeeman shift induced by static field measurements²⁵. Therefore, our technique should better apply to environment with non-characterized or many geometrical configurations of vicinal spins, such as in NV-ensembles. Our results emphasize that the polarization of the central spin surroundings plays a major role in its dynamics.

Acknowledgments

The authors thank Chen Avinadav for fruitful discussions and suggestions. J.R.M acknowledges support from Fondecyt-Conicyt grant No. 1141185, PIA-Conicyt grant No. ACT1108, and US Air Force grant FA9550-15-1-0113.

Appendix: Bath polarization effect on the decoherence properties

An additional effect of the bath polarization on the central spin lays in its *decoherence properties*. When the bath is highly polarized, the coherence time T_2 increases since the deteriorating bath dynamics (flip-flops) is quenched^{12,13}. This effect was measured experimentally in¹³ by varying the temperature at high magnetic fields, allowing an **electronic** spin bath to be polarized thermally. The model suggested in ref¹³ is plotted in Fig.4 (solid blue line) along with the polarization dependence referred in¹⁴, which was applied for an electronic bath as well (dashed black line). The additional marks in Fig.4 represent the $T_{1/2}$ times (the time at which the spin has decohered to half of its initial coherence) obtained from a disjoint cluster method²⁸ that we have performed for a single NV-center surrounded by a bath of **nuclear** spins. Normalizing the coherence times by $T_{1/2}^{(P=0)}$ - the coherence time of an NV center within an unpolarized bath ($T_{1/2}^{(P=0)}$ values for a nuclear bath are given in the inset, and are consistent with²⁸), one defines the *enhancement* in $T_{1/2}$ and forms a universal figure of merit for the bath polarization influence. Circles, triangles, squares and pentagrams, correspond to the enhancement of $T_{1/2}$ for nuclear bath with abundance 0.5%, 1%, 2%, and 3% respectively. In general, refs.^{13,14} and our results show that a significant change in T_2 should be expected only in high degree of polarizations. Our results also indicate that as the bath becomes denser, the flip-flop process becomes stronger and faster, shortening the bare coherence time $T_{1/2}^{(P=0)}$, and also demanding higher degree of polarization to be quenched by. This could settle the different trends presented in¹³ and¹⁴.

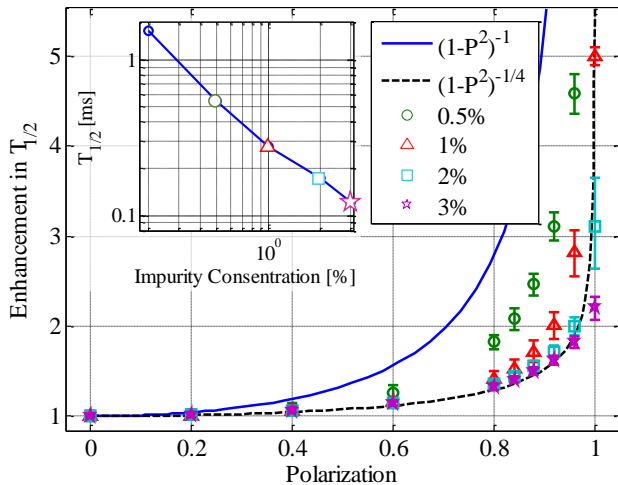


Figure 4: Decoherence properties of a single NV within a polarized spin bath. The increase in $T_{1/2}$ is given as a function of the surrounding bath polarization. The solid blue line corresponds to a $(1 - P^2)^{-1}$ dependence (taken from¹³, and the dashed black line corresponds to a $(1 - P^2)^{-1/4}$ dependence, taken from¹⁴. Inset: $T_{1/2}$ as a function of the abundance for an unpolarized bath ($P = 0$).

- ¹ Cai, J, Retzker, A, Jelezko, F, & Plenio, M. B. (2013) *Nat. Phys.* **9**, 168.
- ² Mamin, H. J, Kim, M, Sherwood, M. H, Rettner, C. T, Ohno, K, Awschalom, D. D, & Rugar, D. (2013) *Science* **339**, 557–560.
- ³ Staudacher, T, Shi, F, Pezzagna, S, Meijer, J, Du, J, Meriles, C. A, Reinhard, F, & Wrachtrup, J. (2013) *Science* **339**, 561–563.
- ⁴ Ajoy, A, Bissbort, U, Lukin, M. D, Walsworth, R. L, & Cappellaro, P. (2015) *Phys. Rev. X* **5**, 011001.
- ⁵ Fischer, R, Bretschneider, C. O, London, P, Budker, D, Gershoni, D, & Frydman, L. (2013) *Phys. Rev. Lett.* **111**, 057601.
- ⁶ Alvarez, G. A, Bretschneider, C, Fischer, R, London, P, Hisao, K, Onada, S, Isoya, J, Gershoni, D, & Frydman, L. (2014) *arXiv:1412.8635*.
- ⁷ Kornack, T. W, Ghosh, R. K, & Romalis, M. V. (2005) *Phys. Rev. Lett.* **95**, 230801.
- ⁸ Walker, T. G & Happer, W. (1997) *Rev. Mod. Phys.* **69**, 629–642.
- ⁹ Makhonin, M. N, Kavokin, K. V, Senellart, P, Lemaître, A, Ramsay, A. J, Skolnick, M. S, & Tartakovskii, A. I. (2011) *Nat Mater* **10**, 844.
- ¹⁰ London, P, Scheuer, J, Cai, J.-M, Schwarz, I, Retzker, A, Plenio, M. B, Katagiri, M, Teraji, T, Koizumi, S, Isoya, J, Fischer, R, McGuinness, L. P, Naydenov, B, & Jelezko, F. (2013) *Phys. Rev. Lett.* **111**, 067601.
- ¹¹ Liu, G.-Q, Jiang, Q.-Q, Chang, Y.-C, Liu, D.-Q, Li, W.-X, Gu, C.-Z, Po, H. C, Zhang, W.-X, Zhao, N, & Pan, X.-Y. (2014) *Nanoscale* **6**, 10134–10139.
- ¹² Zhang, W, Hu, J.-L, Zhuang, J, You, J. Q, & Liu, R.-B. (2010) *Phys. Rev. B* **82**, 045314.
- ¹³ Takahashi, S, Hanson, R, van Tol, J, Sherwin, M. S, & Awschalom, D. D. (2008) *Phys. Rev. Lett.* **101**, 047601.
- ¹⁴ Goldstein, G, Cappellaro, P, Maze, J. R, Hodges, J. S, Jiang, L, Sørensen, A. S, & Lukin, M. D. (2011) *Phys. Rev. Lett.* **106**, 140502.
- ¹⁵ Balasubramanian, G, Neumann, P, Twitchen, D, Markham, M, Kolesov, R, Mizuochi, N, Isoya, J, Achard, J, Beck, J, Tissler, J, Jacques, V, Hemmer, P. R, Jelezko, F, & Wrachtrup, J. (2009) *Nat Mater* **8**, 383.
- ¹⁶ Waldherr, G, Wang, Y, Zaiser, S, Jamali, M, Schulte-Herbruggen, T, Abe, H, Ohshima, T, Isoya, J, Du, J. F, Neumann, P, & Wrachtrup, J. (2014) *Nature* **506**, 204–207.
- ¹⁷ Balasubramanian, G, Chan, I. Y, Kolesov, R, Al-Hmoud, M, Tisler, J, Shin, C, Kim, C, Wojcik, A, Hemmer, P. R, Krueger, A, Hanke, T, Leitenstorfer, A, Bratschitsch, R, Jelezko, F, & Wrachtrup, J. (2008) *Nature* **455**, 648–651.
- ¹⁸ Maze, J. R, Stanwix, P. L, Hodges, J. S, Hong, S, Taylor, J. M, Cappellaro, P, Jiang, L, Dutt, M. V, Gurudev Togan, E, Zibrov, A. S, Yacoby, A, Walsworth, R. L, & Lukin, M. D. (2008) *Nature* **455**, 644–647.
- ¹⁹ Kucsko, G, Maurer, P. C, Yao, N. Y, Kubo, M, Noh, H. J, Lo, P. K, Park, H, & Lukin, M. D. (2013) *Nature* **500**, 54.
- ²⁰ McGuinness, L. P. (2011) *Nat. Nano* **6**, 358.
- ²¹ Hahn, E. (1950) *Phys. Rev.* **80**, 580–594.
- ²² Slichter, C. P, ed. (1990) *Principles of Magnetic Resonance*. (Springer-Verlag, New York), p. 600.
- ²³ Taylor, J. M, Cappellaro, P, Childress, L, Jiang, L, Budker, D, Hemmer, P. R, Yacoby, A, Walsworth, R, & Lukin, M. D. (2008) *Nat. Phys.* **4**, 810.
- ²⁴ (In general, the electronic $|0\rangle$ probability after a ϕ -shifted

- terminating ($\pi/2$) pulse is $p_\phi = \frac{1}{2} (1 + \text{Re} \{e^{i\phi} S\})$.
- ²⁵ (Supplementary information can be found online.)
- ²⁶ Mims, W. (1972) *Phys. Rev. B* **5**, 2409–2419.
- ²⁷ Rowan, L. G, Hahn, E. L, & Mims, W. B. (1965) *Phys. Rev.* **137**, A61–A71.
- ²⁸ Maze, J. R, Taylor, J. M, & Lukin, M. D. (2008) *Phys. Rev. B* **78**, 094303.
- ²⁹ Kolkowitz, S, Unterreithmeier, Q. P, Bennett, S. D, & Lukin, M. D. (2012) *Phys. Rev. Lett.* **109**, 137601.
- ³⁰ Zhao, N, Honert, J, Schmid, B, Klas, M, Isoya, J, Markham, M, Twitchen, D, F, Liu, R, Fedder, H, & Wrachtrup, J. (2012) *Nat. Nano.* **7**, 657.
- ³¹ Taminiiau, T. H, Wagenaar, J. J. T, van der Sar, T, Jelezko, F, Dobrovitski, V. V, & Hanson, R. (2012) *Phys. Rev. Lett.* **109**, 137602.
- ³² Childress, L, Gurudev Dutt, M. V, Taylor, J. M, Zibrov, A. S, Jelezko, F, Wrachtrup, J, Hemmer, P. R, & Lukin, M. D. (2006) *Science* **314**, 281–285.
- ³³ Jiang, L, Dutt, M. V. G, Togan, E, Childress, L, Cappellaro, P, Taylor, J. M, & Lukin, M. D. (2008) *Phys. Rev. Lett.* **100**, 073001.
- ³⁴ Dutt, M. V. G, Childress, L, Jiang, L, Togan, E, Maze, J, Jelezko, F, Zibrov, A. S, Hemmer, P. R, & Lukin, M. D. (2007) *Science* **316**, 1312–1316.
- ³⁵ Shim, J. H, Nowak, B, Niemeyer, I, Zhang, J, Brandao, F. D, & Suter, D. (2013) *arXiv:1307.0257*.
- ³⁶ Reinhard, F, Shi, F, Zhao, N, Rempp, F, Naydenov, B, Meijer, J, Hall, L, Hollenberg, L, Du, J, Liu, R.-B, & Wrachtrup, J. (2012) *Phys. Rev. Lett.* **108**, 200402.
- ³⁷ Jacques, V, Neumann, P, Beck, J, Markham, M, Twitchen, D, Meijer, J, Kaiser, F, Balasubramanian, G, Jelezko, F, & Wrachtrup, J. (2009) *Phys. Rev. Lett.* **102**, 057403.
- ³⁸ Fischer, R, Jarmola, A, Kehayias, P, & Budker, D. (2013) *Phys. Rev. B* **87**, 125207.